Pakistan J. Zool., pp 1-8, 2024. **DOI**: https://dx.doi.org/10.17582/journal.pjz/20240502043333

Aquaporin-9 Aggravates Lipopolysaccharides Induced Acute Lung Injury Via Facilitating M1-Like Macrophage Polarization

Jiajia Wan[1,2], Chi Zhang[3], Xiaodi Li[3], Longkang Liu[3], Linxiu Peng[3,4], Yuejian Liu[2], Yang Qiu[2], Guokai Wu[2], Bo Zhang[3]*, Yan Wang[3]* and Tonghui Ma[3]*

[1]*School of Basic Medical Sciences, Dalian Medical University, Dalian 116044, China*
[2]*Central Laboratory, First Affiliated Hospital of Dalian Medical University, Dalian 116011, China*
[3]*School of Medicine, Nanjing University of Chinese Medicine, Nanjing 210023, China*
[4]*School of Life Science, Liaoning Normal University, Dalian 116029, China*

Article Information
Received 02 May 2024
Revised 08 May 2024
Accepted 16 May 2024
Available online 05 July 2024
(early access)

Authors' Contribution
YW: Conceptualization, visualization, writing- review and editing. JW: Conceptualization, data curation, investigation, methodology, writing - original draft. TM: Conceptualization, funding acquisition, resources, supervision, writing-review and editing. BZ: Data curation, formal analysis, validation, writing review and editing. YL: Methodology, software. YQ: Methodology, project administration. GW and CZ, LL: Data curation, methodology. XL: Investigation, methodology, software. LP: Formal analysis, software.

Key words
Acute lung injury, aquaporin-9, hydrogen peroxide, alveolar macrophages, M1-like polarization, NF-κB signaling

ABSTRACT

Alveolar macrophages (AMs) play a crucial role in orchestrating lung inflammation in acute lung injury (ALI), which largely depends upon M1-like macrophage polarization. However, the underlying regulatory mechanisms remain incompletely elucidated. The present study identified, for the first time, that aquaporin-9 (AQP9) is expressed in AMs and undergoes significant up-regulation following lipopolysaccharides (LPS) administration. *AQP9* gene knockout (*AQP9* KO) mice exhibited markedly attenuated alveolar hemorrhage and interstitial edema in an LPS-induced ALI model compared with wild-type (WT) littermates. The mitigated lung injury in *AQP9* KO mice correlated with significantly alleviated pulmonary inflammation as indicated by significantly reduced immunofluorescent staining of $CD68^+$ macrophages in the lungs, decreased level of the pro-inflammatory cytokine IL-6 and increased level of the anti-inflammatory cytokine IL-10 in the bronchoalveolar lavage fluid (BALF). Concurrently, mRNA levels of *TNF-α* and *IL-1β* were also significantly reduced in the lungs of LPS-induced *AQP9* KO mice. Further investigation revealed that AQP9 deficiency caused defective M1-like polarization of AMs due to reduced import of extracellular hydrogen peroxide (H_2O_2) and impeded activation of NF-κB signaling pathway. Our findings demonstrate that AQP9 facilitates M1-like macrophage polarization by modulating plasma membrane H_2O_2 transport, thereby exacerbating lung inflammation in LPS-induced ALI. The study provides new insights into the regulatory mechanisms of M1-like macrophage polarization in LPS-induced ALI.

INTRODUCTION

Acute lung injury (ALI) and its severe manifestation, acute respiratory distress syndrome (ARDS), are characterized by disruption of alveolar barriers, the onset of pulmonary edema, and rapid infiltration of inflammatory cells. These conditions represent critical inflammatory diseases (Bos and Ware, 2022; Matthay *et al*., 2024). Due to the absence of effective treatments, the mortality rate of ARDS is still high, ranging between 35-55% (Meyer *et al*., 2021). Consequently, there is a critical necessity to identify novel therapeutic targets and develop innovative strategies.

ALI can stem from a variety of pathogenic factors, including severe trauma, sepsis, acute pneumonia, and viral infections, with bacterial infection being a primary culprit (Yang *et al*., 2020). As a principal constituent of gram-negative bacteria's outer membrane, lipopolysaccharides (LPS) frequently serves as a clinically relevant model for ALI in murine models because of its ability to trigger acute inflammatory responses (Lai *et al*., 2023). Upon entry into the body, LPS initially activates alveolar macrophages (AMs), which subsequently instigate innate immune responses by generating inflammatory cytokines (Aegerter *et al*., 2022). AMs play a pivotal role in activating local pro-inflammatory networks and inducing lung injury through the release of various cytokines and generation of reactive oxygen species (ROS) after M1 polarization (Cheng *et al*., 2021; Yang *et al*., 2020). The mechanisms

* Corresponding author: zhangbo@njucm.edu.cn, wangyan2020@njucm.edu.cn, matonghui@njucm.edu.cn
0030-9923/2024/0001-0001 $ 9.00/0

underlying the macrophage polarization during ALI are not fully understood.

Aquaporins (AQPs) is a family of transmembrane channel proteins with 13 members. They primarily facilitate water transport and play diverse cellular roles, such as modulation of fluid transport, cell morphology, volume and motility (Login and Nejsum, 2023). AQP9, the most abundant aquaporin in human macrophages, is referred to as a peroxiporin due to its efficient transport of hydrogen peroxide (H_2O_2) across cell membranes (Watanabe *et al*., 2016). Our recent studies have demonstrated that deletion of AQP9 in mice significantly diminishes the export of excessive intracellular H_2O_2 in proliferating hepatocytes, thereby promoting liver regeneration (Li *et al*., 2024; Zhang *et al*., 2022). In macrophages, H_2O_2 is primarily generated by NADPH oxidase 2 (NOX2) at the outer leaflet of the plasma membrane and must traverse a lipid bilayer to reach its cytosolic targets, including the NF-κB transcription factor (Bode *et al*., 2023; Lei *et al*., 2023). Cytosolic H_2O_2 is crucial for the induction and maintenance of M1-like macrophage polarization, which is characterized by activation of the NF-κB signaling pathway and production of pro-inflammatory cytokines (Engur *et al*., 2023; Rendra *et al*., 2019). However, the role of AQP9 in macrophage polarization in ALI is still unclear.

By using an *AQP9*-knockout mouse model, we found that AQP9 facilitates M1-like macrophage polarization by modulating H_2O_2 transport, thereby exacerbating lung inflammation in LPS-induced ALI. The study may provide new insights into the regulatory mechanisms of M1-like macrophage polarization in ALI and ARDS.

MATERIALS AND METHODS

ALI mouse model

AQP9-tdTomato transgenic mice (*AQP9*-RFP, C57BL/6J background) were generated by Shanghai Model Organisms Center, Inc. (Shang hai, China), while *AQP9* gene knockout mice (*AQP9* KO, C57BL/6J background) were genetically modified in Beijing Yishanhengye Biotechnology Co., Ltd. (Beijing, China). The housing conditions are described in the supplementary material.

For LPS-induced ALI model, 8-week-old male WT and *AQP9* KO mice were given 5 mg/kg LPS (Sigma-Aldrich, USA) dissolved in 50 μL of sterile PBS intratracheally or given equal volume of PBS (sham group). Under isoflurane anesthesia, blood and tissue samples were obtained at days 1, 3, and 6 post-LPS administration for subsequent biochemical analysis.

Bronchoalveolar lavage fluid (BALF) collection and cell counts

The BALF sample was obtained following well-established procedures (Zhong *et al*., 2019) as described earlier. To summarize, the lungs of the mice were lavaged three times with 0.5 mL of PBS. Subsequently, the recovered fluid was centrifuged and the resulting supernatant was stored at -80°C for future experiments. The protein content in the BALF was quantified using the BCA assay. The cell pellets were resuspended in 500 μL of PBS, and cell counts were performed using a hemocytometer.

Cell culture

Primary mouse alveolar macrophages (AMs) and neutrophils were isolated and cultured according to established protocols (Yang *et al*., 2020; Zhang *et al*., 2020). AMs were obtained from alveolar lavage fluid and neutrophils were isolated from the peripheral blood of mice by using the Mouse Peripheral Blood Neutrophil Cells Isolation Kit (Solarbio, China) according to the protocols. The detailed methods of cell culture are described in the supplementary material.

Histological analysis

Lung specimens underwent fixation with 4% paraformaldehyde and then paraffin embedding. The methods of hematoxylin and eosin (H&E), immunohistochemical (IHC) staining and immunofluorescence analysis are described in the supplementary material. The degree of lung tissue injury was categorized into grades 0–4 as previously described (Zhao *et al*., 2020).

Immunocytochemistry

AMs cultured on coverslips were treated with either 500 ng/mL LPS (Sigma-Aldrich, USA) or not for 48 h. Following fixation and permeabilization, cells were blocked with 1% BSA for 30 min. The primary antibodies targeting F4/80 (1:50, Santa Cruz, sc-377009, USA), CD206 (1:100, Arigo, ARG22456, China), and CD86 (1:200, Arigo, ARG42635, China) were applied overnight, followed by incubation with secondary antibodies labeled with fluorescent dyes for 1 h. Images were acquired using a Leica DM2500 fluorescence microscope, with consistent exposure settings and laser gain for each condition.

HyPerRed fluorescence imaging

HyPerRed (BrainVTA, China), a lentivirus carrying the H_2O_2-sensitive fluorescent protein, was utilized to transfect primary cultured cells and detect hydrogen peroxide in the cytosol of living cells as previously described (Lyublinskaya and Antunes, 2019). HyPerRed was transfected into AMs derived from WT and *AQP9*

KO mice, whereas a lentivirus without HyPerRed was transfected into AMs as a control group. Finally, cytoplasmic HyPerRed fluorescence was measured using a confocal laser scanning microscope (Leica, SP8 DIVE, Germany) following 72 h of incubation.

RT-qPCR analysis

RNA was extracted from tissues and purified cells using TRIZOL reagent (Vazyme, China). cDNA was obtained via the reverse transcription using commercial kits (Accurate Biology, China). RT-qPCR analysis was carried out with SYBR Green PCR master mix (Accurate Biology, China). The expression levels of target genes were normalized to β-actin levels. Details of the primers utilized can be found in the supplementary information.

Western blot analysis

RIPA lysis buffer containing protease inhibitor cocktail (Beyotime, China) were used to lyse cells and tissues. Proteins in the lysates were separated by SDS-PAGE, transferred to PVDF membranes and probed using indicated antibodies. Nuclear extract was prepared with a commercial kit (Thermo Fisher Scientific, USA) according to the instructions. The antibodies used for western blot are provided in the supplementary material.

Enzyme-linked immunosorbent assay (ELISA)

The levels of IL-6 and IL-10 in mouse BALF and culture supernatant of AMs after LPS adminisration were detected by ELISA kits (Elabscience, USA) according to the instructions. Absorbance was measured at 450 nm using a microplate reader.

Statistical analysis

GraphPad Prism 8.0 (GraphPad Software, USA) was used for statistical analyses. Student's t-test was employed for comparisons between two groups, while two-way ANOVA was utilized to compare multiple groups with multiple variables. All data are presented as mean±SEM. A *P*-value of less than 0.05 was considered statistically significant for all tests.

RESULTS

LPS induces AQP9 *expression in macrophages*

Since AMs and neutrophils are known to be crucial in orchestrating inflammatory responses during ALI (Bos and Ware, 2022; Matthay *et al*., 2024), we firstly investigated the expression of *AQP* 0-12 in AMs and neutrophils isolated from C57BL/6J mice. As depicted in Figure 1A, the most abundant *AQP* in AMs is *AQP9*, which is also expressed in neutrophils. We futher found that *AQP9* mRNA expression exhibited a significant increase in murine AMs following stimulation with LPS, but *AQP9* expression in neutrophils was not increased after LPS treatment (Fig. 1B). Correspondingly, AQP9 protein expression was augmented in LPS-treated AMs (Fig. 1C). Then we utilized *AQP9* -tdTomato (*AQP9* -RFP) mice to validate AQP9 expression in AMs. Fluorescence imaging revealed a marked up-regulation of *AQP9* in LPS-stimulated AMs of AQP9-RFP mice compared to the control group (Fig. 1D). Collectively, up-regulation of AQP9 expression in AMs upon LPS induction suggests its involvement in the pathogenesis of infectious ALI.

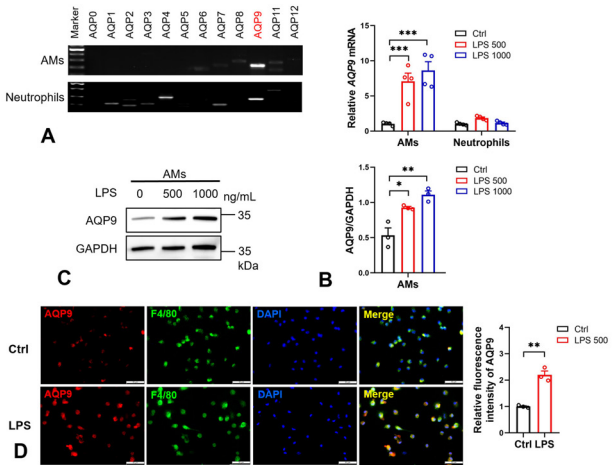

Fig. 1. AQP9 expression is up-regulated in AMs after LPS stimulation. (**A**) Representative PCR amplification analysis of *AQP9* 0-12 in AMs and neutrophils isolated from C57BL/6J mice. (**B**) mRNA levels of *AQP9* in LPS-treated (500 or 1000 ng/mL) AMs and neutrophils were assessed by RT-qPCR (n = 4). (**C**) Western blot analysis of AQP9 in LPS-treated (500 or 1000 ng/mL) AMs (n = 3). (**D**) Representative fluorescence images of AQP9 (red) and macrophage marker F4/80 (green) and quantification of AQP9 in LPS-treated (500 ng/mL) AMs isolated from male *AQP9*-RFP mice (n = 3). Scale bars, 50 μm. Data are expressed as mean ± SEM. $^{*}P < 0.05$, $^{**}P < 0.01$, $^{***}P < 0.001$, Student's t-test for two-group comparisons, two-way ANOVA for comparisons with multiple variables.

AQP9 *deficiency attenuates pulmonary inflammation and lung injury in LPS-induced ALI*

To investigate the involvement of AQP9 in the pathogenesis of ALI, we employed an LPS-induced ALI using *AQP9* KO mice and WT littermates as control. Both WT and *AQP9* KO mice were intratracheally instilled with 5 mg/kg LPS. H&E staining revealed that LPS induced marked pathological changes, characterized by increased inflammatory cell infiltration, alveolar hemorrhage, interstitial edema, and heightened alveolar wall thickness

at days 1, 3, and 6 post-surgery (Fig. 2A). In comparison to WT littermates, *AQP9* KO mice exhibited significantly mitigated lung damage and reduced lung injury scores at the corresponding time points post-surgery (Fig. 2A, B). Moreover, LPS-induced *AQP9* KO mice demonstrated decreased lung Wet/Dry (W/D) weight ratio (Fig. 2C), indicating reduced pulmonary edema, along with diminished counts of inflammatory cells in BALF (Fig. 2D). Additionally, protein leakage in the BALF of LPS-challenged *AQP9* KO mice was notably lower than that in WT control (Fig. 2E). Furthermore, AQP9 deficiency resulted in a decreased level of the pro-inflammatory cytokine IL-6, while increasing the level of the anti-inflammatory cytokine IL-10 in BALF (Fig. 2F).

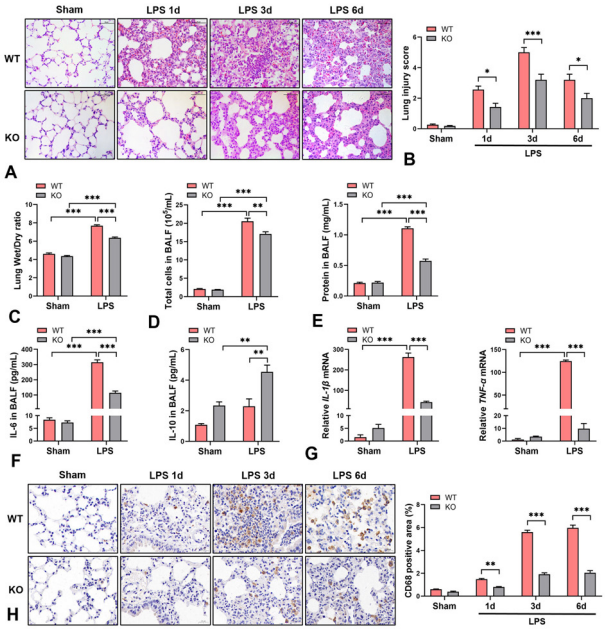

Fig. 2. Effect of AQP9 deletion on LPS-induced ALI and pulmonary inflammation. (A, B, H) *AQP9* KO and WT mice were intratracheally instilled with LPS (5 mg/kg), then sacrificed at days 1, 3, and 6 after surgery for functional analysis. (**A**) Representative images and (**B**) lung injury score analysis of H&E staining of lung tissues (n = 5). Scale bars, 50 μm. (C-G) Male WT and *AQP9* KO mice were sacrificed at day 3 after LPS (5 mg/kg) administration for functional analysis. (**C**) Pulmonary Wet/Dry weight ratio (n = 3). (**D**) Quantity of inflammatory cells in BALF (n = 5). (**E**) Total protein content in BALF (n = 3). (**F**) Concentration of IL-6 and IL-10 in BALF (n = 3). (**G**) mRNA levels of *IL-1β* and *TNF-α* in lung tissues (n = 3). (**H**) Representative $CD68^+$ staining and quantitative analysis in cross-sections of lung tissues (n = 3). Scale bars, 20 μm. Data are expressed as mean ± SEM. $^*P < 0.05$, $^{**}P < 0.01$, $^{***}P < 0.001$, two-way ANOVA for comparisons with multiple variables.

Concurrently, the pro-inflammatory cytokines of *TNF-α* and *IL-1β* in lung tissues of LPS-induced *AQP9* KO mice were significantly reduced compared to WT control mice (Fig. 2G). IHC analysis revealed a significant reduction in $CD68^+$ macrophages in the lungs of LPS-induced *AQP9* KO mice compared with the WT control group (Fig. 2H). In summary, these findings suggest that AQP9 deficiency may alleviate LPS-induced ALI and inflammatory responses in the lungs.

AQP9 *deficiency suppresses M1-like macrophage polarization*

Following this, we investigated how macrophage-mediated inflammation is affected by AQP9. Immunofluorescence staining revealed a significant decrease in $iNOS^+$ macrophages (M1 subtype) in *AQP9* KO lungs at day 3 post-LPS instillation (Fig. 3A). Consistently, *in vitro* experiments demonstrated significantly lower *iNOS* mRNA levels in *AQP9* KO AMs compared to WT AMs after LPS stimulation, while the levels of the M2 macrophage-associated marker *CD206* remained similar between *AQP9* KO and WT AMs (Fig. 3C). Moreover, CD86, another marker of M1 macrophages, exhibited markedly reduced expression in LPS-treated *AQP9* KO vs. WT AMs, whereas CD206 expression showed no significant change (Fig. 3B). Additionally, the level of IL-6 was down-regulated, while IL-10 level was increased in the culture media of LPS-treated *AQP9* KO AMs compared to WT AMs (Fig. 3D). Furthermore, AQP9 deletion led to decreased expression of *IL-6* and *IL-1β*, alongside up-regulation of *IL-10* expression in AMs (Fig. 3E). These findings suggest that AQP9 deficiency may alleviate inflammatory responses in LPS-induced ALI by inhibiting M1-like macrophage polarization.

AQP9 *promotes M1-like polarization of macrophages by regulating* H_2O_2 *transport*

Finally, we investigated the molecular mechanisms involved in AQP9 modulating macrophage polarization. We postulated that AQP9-mediated H_2O_2 transport may play a key role in M1/M2 macrophage polarization and inflammatory responses. Given that activated NOX2 is the main producer of H_2O_2 in LPS-stimulated macrophages, we first confirmed the up-regulation of NOX2 in LPS-treated AMs (Fig. 4A). Subsequently, we assessed the intra- and extracellular levels of H_2O_2 in AMs following LPS administration. AQP9 deficiency notably reduced the intracellular level of H_2O_2 in LPS-treated AMs (Fig. 4B), whereas significantly increased the extracellular content of H_2O_2 in the culture media of AMs post-LPS stimulation (Fig. 4C). To precisely track the cytoplasmic H_2O_2 level in AMs, we utilized live cell imaging with a lentivirus-transduced H_2O_2-sensitive

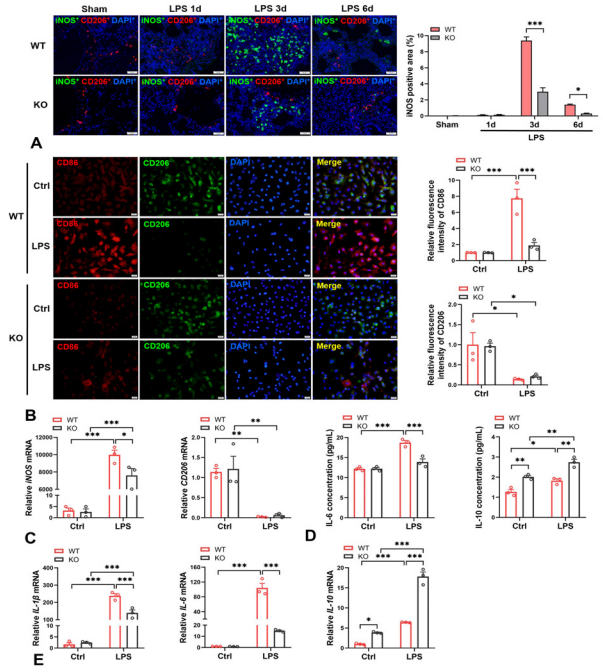

Fig. 3. Effect of AQP9 deletion on M1-like macrophage polarization in vivo and ex vivo. (**A**) Representative immunofluorescence images of iNOS (green) and CD206 (red) and quantification of iNOS$^+$ areas in the lung tissues of WT and *AQP9* KO mice at days 1, 3, and 6 after LPS intratracheal instillation (5 mg/kg) (n = 6). Scale bars, 50 μm. (B-E) AMs isolated from WT and *AQP9* KO mice were stimulated with LPS (500 ng/mL) for 24 h. (**B**) Representative immunofluorescence images and quantification of CD86 (red) and CD206 (green) in AMs (n = 3). Scale bars, 20 μm. (**C**) mRNA levels of *iNOS* and *CD206* in AMs were assessed by RT-qPCR (n = 3). (**D**) The levels of IL-6 and IL-10 in the culture media of AMs were determined by ELISA (n = 3). (**E**) mRNA levels of *IL-1β, IL-6* and *IL-10* in AMs (n = 3). Data are presented as mean ± SEM. $^*P < 0.05$, $^{**}P < 0.01$, $^{***}P < 0.001$, two-way ANOVA for comparisons with multiple variables.

fluorescent protein HyPerRed. As depicted in Figure 4D, the cytoplasmic H_2O_2 level was markedly higher in WT AMs compared to *AQP9* KO AMs after LPS stimulation, although this elevation in WT AMs was mitigated by H_2O_2 inhibitor N-acetylcysteine (NAC). Furthermore, the capacity of *AQP9* KO AMs to uptake exogenous H_2O_2 was significantly decreased compared to WT AMs (Fig. 4E).

Considering that H_2O_2 in the cytoplasm can activate the NF-κB signaling pathway and promote the polarization of M1-like macrophages, thereby initiating the expression of most pro-inflammatory genes, we explored the relationship between AQP9 and the NF-κB signaling pathway. Western blot analysis revealed that AQP9 deficiency substantially reduced the phosphorylation of IKK and p65, as well as IκBα degradation in LPS-treated AMs (Fig. 4F, G). Moreover, we observed a decreased nuclear translocation of p65 in LPS-treated *AQP9* KO vs. WT AMs (Fig. 4H, I). Thus, our findings indicate that AQP9 may activate the NF-κB pathway by increasing the uptake of H_2O_2, ultimately leading to M1-like macrophage polarization.

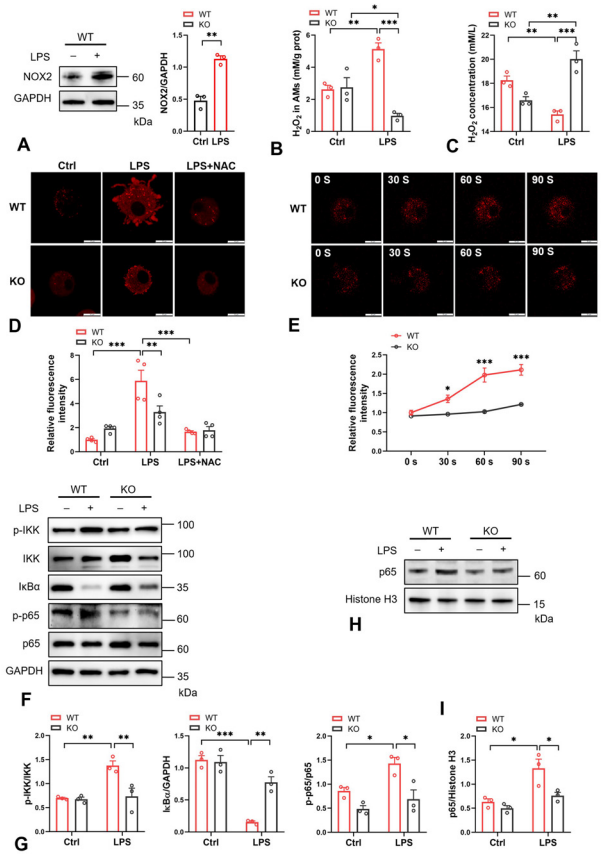

Fig. 4. Effect of AQP9 deletion on the H_2O_2/NF-κB axis in AMs. AMs isolated from WT and *AQP9* KO mice were treated with LPS (500 ng/mL) for 4 h. (**A**) Western blot analysis of NOX2 in WT AMs (n=3). (**B**) Intracellular H_2O_2 content in WT and *AQP9* KO AMs (n=3). (**C**) Extracellular H_2O_2 levels in the culture media of AMs (n=3). (**D**) Representative fluorescent images and quantitative analysis of HyPerRed-transduced WT and *AQP9* KO AMs cultured with or without LPS or NAC (2.5 mM) for 4 h (n=3). Scale bars, 10 μm. (**E**) Representative fluorescent images and quantification of HyPerRed-transduced WT and *AQP9* KO AMs incubated with 100 μM H_2O_2 (n=3). Scale bars, 10 μm. (**F**, **G**) Western blot analysis of p-IKK, IKK, IκBα, p-p65, and p65 in LPS-treated AMs (n=3). (**H**, **I**) Western blot analysis of nuclear extracts prepared from AMs and analyzed for p65 and Histone H3 (n=3). Data are expressed as mean ± SEM. $^*P < 0.05$, $^{**}P < 0.01$, $^{***}P < 0.001$, two-way ANOVA for comparisons with multiple variables.

DISCUSSION

Pulmonary and systemic inflammation are hallmark features of ALI and ARDS, contributing to the progression of these conditions by exacerbating pulmonary insults (Bos and Ware, 2022; Matthay *et al*., 2024). AMs and neutrophils both play pivotal roles in pulmonary inflammation, releasing various cytokines and ROS, including H_2O_2 (Meyer *et al*., 2021; Yang *et al*., 2020). Although the correlation between AQP9 and various immune infiltrating cells, including macrophages, has been documented in previous studies (Liu *et al*., 2020, 2023; Matsushima *et al*., 2014), the present study provided first evidence demonstrating the expression of AQP9 in AMs, which is substantially up-regulated following LPS stimulation. Nevertheless, we found that AQP9 expression in neutrophils was not increased after LPS treatment. Thus, we mainly investigated the role and mechanism of AQP9 in AMs on the regulation of LPS-induced ALI.

Our study suggests that AQP9 serves as a significant contributor to the pro-inflammatory signaling driving the development of ALI, as indicated by its up-regulation following LPS stimulation and the alleviation of pulmonary inflammation upon its transgenic deletion. Three key findings from our study support the important role of AQP9 in the development of ALI. First, the absence of AQP9 substantially lessened lung damage resulting from LPS exposure in mice. Secondly, levels of pro-inflammatory mediators were markedly reduced in BALF and lung tissues of *AQP9* knockout mice. Third, deletion of AQP9 prominently suppressed the NF-κB signaling pathway and M1-like polarization of macrophages. Together, these findings underscore AQP9 as a potential therapeutic target for ALI due to its pro-inflammatory properties.

AQP9 has become increasingly recognized as a crucial modulator of cellular homeostasis for H_2O_2 and regulating function by promoting the diffusion of H_2O_2 through cellular membranes. Studies have demonstrated that AQP9 overexpression potentiated the cellular increase in H_2O_2 levels upon the addition of exogenous H_2O_2 in Chinese hamster ovary-K1 cells, while AQP9 knockdown reduces extracellular H_2O_2 entry in human liver cancer HepG2 cells (Watanabe *et al*., 2016). Similarly, erythrocytes from *AQP9* knockout mice showed suppressed uptake of extracellular H_2O_2 compared to WT cells (Kucherenko *et al*., 2012). Our previous work has highlighted the critical role of AQP9 in mediating H_2O_2 transport across plasma membrane in hepatocytes, where AQP9-mediated H_2O_2 export alleviates oxidative stress and facilitates liver regeneration after hepatectomy (Li *et al*., 2024; Zhang *et al*., 2022).

Based on these findings, our study is the first to demonstrate that AQP9 facilitates the efficient uptake of H_2O_2 across plasma membranes in AMs. By utilizing a cytoplasmic H_2O_2-sensitive fluorescent protein, we observed a significant reduction in cytoplasmic H_2O_2 levels in *AQP9*-deficient AMs compared to wild-type AMs following LPS stimulation. Previous studies have implicated ROS-generating NADPH oxidases, particularly NOX2, in LPS-induced lung inflammation, with NOX2 serving as a major source of inflammation-associated ROS production in macrophages (Kouki *et al*., 2023; Sul and Ra, 2021; Zhong *et al*., 2019). Upon activation, NOX2 generates superoxide, which is rapidly converted to H_2O_2 either intracellularly or extracellularly. We observed that AQP9 deficiency reduced the import of exogenous H_2O_2 in AMs, providing further confirmation of AQP9's role in transporting H_2O_2 across membranes in AMs. It is well established that cytosolic H_2O_2 can activate the NF-κB pathway by mediating the activation of inhibitor of NF-κB (IκB) kinases, which regulate the stability of IκB (Bode *et al*., 2023). Mounting evidence has implicated AQP9 in NF-κB pathway activation in septic models (Mohammad *et al*., 2022; Tesse *et al*., 2021). Our results showed that the loss of AQP9 strongly inhibited M1-like macrophage polarization both *in vivo* and *ex vivo*, while the expression of the M2 macrophage marker CD206 remained unaffected. Additionally, AQP9 deficiency significantly attenuated NF-κB pathway activation in LPS-treated AMs. These findings suggest that AQP9 may promote M1-like polarization of macrophages by facilitating the uptake of extracellular H_2O_2 derived from NOX2 activation and subsequently activating the NF-κB pathway.

However, it is crucial to notice that there exist conflicting findings in alternative research. For example, Shi *et al*. (2022) and Jing *et al*. (2021) reported that AQP9 stimulates an M2-like polarization in tumor-associated macrophages. We speculate that this discrepancy may be attributed to differences in cell types and disease models. The diverse roles of AQP9 in regulating macrophage polarization may indeed be influenced by various disease microenvironments, and the underlying mechanisms require further study.

CONCLUSIONS

In summary, the study implicates a key role of AQP9 in facilitating M1-like polarization of AMs via modulating plasma membrane H_2O_2 transport, thereby exacerbating lung inflammation in LPS-induced ALI. The study will hopefully provide new target and develop innovative strategy for ALI and ARDS.

DECLARATIONS

Acknowledgement

We appreciate Nanjing University of Chinese Medicine for its support of this project. Moreover, we are grateful to the central laboratory's staff of the First Affliated Hospital of Dalian Medical University who helped us in performing the present project.

Funding

This study was supported by the National Natural Science Foundation of China (grant numbers: 82073913, 82374013).

Ethical statement and IRB approval

The animal study protocol was approved by the Institutional Animal Care and Use Committee of Nanjing University of Chinese Medicine (Approval No. 202202A044).

Supplementary material

There is supplementary material associated with this article, available at https://dx.doi.org/10.17582/journal.pjz/20240502043333.

Statement of conflict of interest

The authors have declared no conflicts of interest.

REFERENCES

Aegerter, H., Lambrecht, B.N. and Jakubzick, C.V., 2022. Biology of lung macrophages in health and disease. *Immunity*, **55:** 1564-1580. https://doi.org/10.1016/j.immuni.2022.08.010

Bode, K., Hauri-Hohl, M., Jaquet, V. and Weyd, H., 2023. Unlocking the power of NOX2: A comprehensive review on its role in immune regulation. *Redox Biol.*, **64:** 102795. https://doi.org/10.1016/j.redox.2023.102795

Bos, L.D.J. and Ware, L.B., 2022. Acute respiratory distress syndrome: Causes, pathophysiology, and phenotypes. *Lancet*, **400:** 1145-1156. https://doi.org/10.1016/S0140-6736(22)01485-4

Cheng, P., Li, S. and Chen, H., 2021. Macrophages in lung injury, repair, and fibrosis. *Cells*, **10:** 436. https://doi.org/10.3390/cells10020436

Engur, D., Ercan, I., Kiser, C., Tufekci, K.U., Soy, S., Micili, S.C., Ozhan, G., Guven, S., Kumral, A. and Genc, S., 2023. Hydrogen peroxide signaling modulates neuronal differentiation via microglial polarization and Wnt/β-catenin pathway. *Eur. Rev. Med. Pharmacol. Sci.*, **27:** 5083-5096.

Jing, J., Sun, J., Wu, Y., Zhang, N., Liu, C., Chen, S., Li, W., Hong, C., Xu, B. and Chen, M., 2021. AQP9 is a prognostic factor for kidney cancer and a promising indicator for M2 TAM polarization and CD8+ T-cell recruitment. *Front. Oncol.*, **11:** 770565. https://doi.org/10.3389/fonc.2021.770565

Kouki, A., Ferjani, W., Ghanem-Boughanmi, N., Ben-Attia, M., Dang, P. M., Souli, A. and El-Benna, J., 2023. The NADPH oxidase inhibitors apocynin and diphenyleneiodonium protect rats from LPS-induced pulmonary inflammation. *Antioxidants* (Basel), **12:** 770. https://doi.org/10.3390/antiox12030770

Kucherenko, Y.V., Huber, S.M., Nielsen, S. and Lang, F., 2012. Decreased redox-sensitive erythrocyte cation channel activity in aquaporin 9-deficient mice. *J. Membr. Biol.*, **245:** 797-805. https://doi.org/10.1007/s00232-012-9482-y

Lai, K., Song, C., Gao, M., Deng, Y., Lu, Z., Li, N. and Geng, Q., 2023. Uridine alleviates sepsis-induced acute lung injury by inhibiting ferroptosis of macrophage. *Int. J. mol. Sci.*, **24:** 5093. https://doi.org/10.3390/ijms24065093

Lei, L., Zhang, F., Huang, J., Yang, X., Zhou, X., Yan, H., Chen, C., Zheng, S., Si, L., Jose, P. A., Zeng, C. and Yang, J., 2023. Selenium deficiency causes hypertension by increasing renal AT(1) receptor expression via GPx1/H(2)O(2)/NF-κB pathway. *Free Radic. Biol. Med.*, **200:** 59-72. https://doi.org/10.1016/j.freeradbiomed.2023.02.021

Li, Y., Yang, X., Bao, T., Sun, X., Li, X., Zhu, H., Zhang, B. and Ma, T., 2024. Radix Astragali decoction improves liver regeneration by upregulating hepatic expression of aquaporin-9. *Phytomedicine*, **122:** 155166. https://doi.org/10.1016/j.phymed.2023.155166

Liu, W., Li, Y., Zhang, Y., Li, S., Chen, Y., Han, B. and Lu, Y., 2023. Identification of biomarkers and immune infiltration in acute myocardial infarction and heart failure by integrated analysis. *Biosci. Rep.*, **43:** BSR20222552. https://doi.org/10.1042/BSR20222552

Liu, X., Xu, Q., Li, Z. and Xiong, B., 2020. Integrated analysis identifies AQP9 correlates with immune infiltration and acts as a prognosticator in multiple cancers. *Sci. Rep.*, **10:** 20795. https://doi.org/10.1038/s41598-020-77657-z

Login, F.H. and Nejsum, L.N., 2023. Aquaporin water channels: Roles beyond renal water handling. *Nat. Rev. Nephrol.*, **19:** 604-618. https://doi.org/10.1038/s41581-023-00734-9

Lyublinskaya, O. and Antunes, F., 2019. Measuring

intracellular concentration of hydrogen peroxide with the use of genetically encoded H_2O_2 biosensor HyPer. *Redox Biol.*, **24:** 101200. https://doi.org/10.1016/j.redox.2019.101200

Matsushima, A., Ogura, H., Koh, T., Shimazu, T. and Sugimoto, H., 2014. Enhanced expression of aquaporin 9 in activated polymorphonuclear leukocytes in patients with systemic inflammatory response syndrome. *Shock*, **42:** 322-326. https://doi.org/10.1097/SHK.0000000000000218

Matthay, M.A., Arabi, Y., Arroliga, A.C., Bernard, G., Bersten, A.D., Brochard, L.J., Calfee, C.S., Combes, A., Daniel, B.M., Ferguson, N.D., Gong, M.N., Gotts, J.E., Herridge, M.S., Laffey, J.G., Liu, K.D., Machado, F.R., Martin, T.R., McAuley, D.F., Mercat, A., Moss, M., Mularski, R.A., Pesenti, A., Qiu, H., Ramakrishnan, N., Ranieri, V.M., Riviello, E.D., Rubin, E., Slutsky, A.S., Thompson, B.T., Twagirumugabe, T., Ware, L.B. and Wick, K.D., 2024. A new global definition of acute respiratory distress syndrome. *Am. J. Respir. Crit. Care Med.*, **209:** 37-47. https://doi.org/10.1164/ajrccm-conference.2023.207.1_MeetingAbstracts.A6229

Meyer, N.J., Gattinoni, L. and Calfee, C.S., 2021. Acute respiratory distress syndrome. *Lancet*, **398:** 622-637. https://doi.org/10.1016/S0140-6736(21)00439-6

Mohammad, S., O'Riordan, C.E., Verra, C., Aimaretti, E., Alves, G.F., Dreisch, K., Evenäs, J., Gena, P., Tesse, A., Rützler, M., Collino, M., Calamita, G. and Thiemermann, C., 2022. RG100204, a novel aquaporin-9 inhibitor, reduces septic cardiomyopathy and multiple organ failure in murine sepsis. *Front. Immunol.*, **13:** 900906. https://doi.org/10.3389/fimmu.2022.900906

Rendra, E., Riabov, V., Mossel, D.M., Sevastyanova, T., Harmsen, M.C. and Kzhyshkowska, J., 2019. Reactive oxygen species (ROS) in macrophage activation and function in diabetes. *Immunobiology*, **224:** 242-253. https://doi.org/10.1016/j.imbio.2018.11.010

Shi, Y., Yasui, M. and Hara-Chikuma, M., 2022. AQP9 transports lactate in tumor-associated macrophages to stimulate an M2-like polarization that promotes colon cancer progression. *Biochem. Biophys. Rep.*, **31:** 101317. https://doi.org/10.1016/j.bbrep.2022.101317

Sul, O.J. and Ra, S.W., 2021. Quercetin prevents LPS-induced oxidative stress and inflammation by modulating NOX2/ROS/NF-kB in lung epithelial cells. *Molecules*, **26:** 6949. https://doi.org/10.3390/molecules26226949

Tesse, A., Gena, P., Rützler, M. and Calamita, G., 2021. Ablation of aquaporin-9 ameliorates the systemic inflammatory response of LPS-induced endotoxic shock in mouse. *Cells*, **10:** 435. https://doi.org/10.3390/cells10020435

Watanabe, S., Moniaga, C.S., Nielsen, S. and Hara-Chikuma, M., 2016. Aquaporin-9 facilitates membrane transport of hydrogen peroxide in mammalian cells. *Biochem. biophys. Res. Commun.*, **471:** 191-197. https://doi.org/10.1016/j.bbrc.2016.01.153

Yang, H.H., Duan, J.X., Liu, S.K., Xiong, J.B., Guan, X.X., Zhong, W.J., Sun, C.C., Zhang, C.Y., Luo, X.Q., Zhang, Y.F., Chen, P., Hammock, B.D., Hwang, S.H., Jiang, J.X., Zhou, Y. and Guan, C.X., 2020. A COX-2/sEH dual inhibitor PTUPB alleviates lipopolysaccharide-induced acute lung injury in mice by inhibiting NLRP3 inflammasome activation. *Theranostics*, **10:** 4749-4761. https://doi.org/10.7150/thno.43108

Zhang, B., Lv, D., Chen, Y., Nie, W., Jiao, Y., Zhang, J., Zhou, X., Wu, X., Chen, S. and Ma, T., 2022. Aquaporin-9 facilitates liver regeneration following hepatectomy. *Redox Biol.*, **50:** 102246. https://doi.org/10.1016/j.redox.2022.102246

Zhang, L., Cheng, Q., Li, C., Zeng, X. and Zhang, X.Z., 2020. Near infrared light-triggered metal ion and photodynamic therapy based on AgNPs/porphyrinic MOFs for tumors and pathogens elimination. *Biomaterials*, **248:** 120029. https://doi.org/10.1016/j.biomaterials.2020.120029

Zhao, Y., Jiang, Y., Chen, L., Zheng, X., Zhu, J., Song, X., Shi, J., Li, Y. and He, W., 2020. Inhibition of the endoplasmic reticulum (ER) stress-associated IRE-1/XBP-1 pathway alleviates acute lung injury via modulation of macrophage activation. *J. Thorac. Dis.*, **12:** 284-295. https://doi.org/10.21037/jtd.2020.01.45

Zhong, W. J., Yang, H.H., Guan, X.X., Xiong, J.B., Sun, C.C., Zhang, C.Y., Luo, X.Q., Zhang, Y.F., Zhang, J., Duan, J.X., Zhou, Y. and Guan, C.X., 2019. Inhibition of glycolysis alleviates lipopolysaccharide-induced acute lung injury in a mouse model. *J. cell. Physiol.*, **234:** 4641-4654. https://doi.org/10.1002/jcp.27261

Pakistan J. Zool., vol. XX(0), pp 000-000, 2024 **DOI**: https://dx.doi.org/10.17582/journal.pjz/20240502043333

Supplementary Material

Aquaporin-9 Aggravates Lipopolysaccharides Induced Acute Lung Injury Via Facilitating M1-Like Macrophage Polarization

Jiajia Wan[1,2], Chi Zhang[3], Xiaodi Li[3], Longkang Liu[3], Linxiu Peng[3,4], Yuejian Liu[2], Yang Qiu[2], Guokai Wu[2], Bo Zhang[3]*, Yan Wang[3]* and Tonghui Ma[3]*

[1]School of Basic Medical Sciences, Dalian Medical University, Dalian 116044, China
[2]Central Laboratory, First Affiliated Hospital of Dalian Medical University, Dalian 116011, China
[3]School of Medicine, Nanjing University of Chinese Medicine, Nanjing 210023, China
[4]School of Life Science, Liaoning Normal University, Dalian 116029, China

MATERIALS AND METHODS

ALI mouse model

Male wild-type (WT) and *AQP9* KO mice aged 6 to 8 weeks were utilized (three to five mice per group), sourced from mating pairs of *AQP9* heterozygous parents, and housed in a specific pathogen-free (SPF) facility at Nanjing University of Chinese Medicine. The mice were maintained on standard chow and provided ad libitum access to water, unless otherwise specified, in an environment with a 12-hour light/dark cycle.

Cell culture

AMs were obtained from mouse alveolar lavage fluid, washed with PBS, and resuspended in RPMI 1640 medium (Solarbio, China) containing 10% FBS (Gibco, USA), supplemented with 1% penicillin/streptomycin (Gibco, USA). After 4–6 h of incubation at 37°C with 5% CO_2, nonadherent cells were removed, and the remaining adherent cells were cultured. Neutrophils were isolated from the peripheral blood of C57BL/6J mice (male) using the Mouse Peripheral Blood Neutrophil Cells Isolation Kit. Briefly, the blood samples were collected and centrifugated using neutrophils separation solution (800 g, 25 min) to get different layers of cells. Then the neutrophils were carefully removed from the tube and centrifuged at 250 g for 10 min. The sedimented cell pellets were washed with PBS and resuspended in RPMI 1640 medium containing 10% FBS and 1% penicillin/streptomycin.

Histological analysis

For histological examination, 3 μm thick slices were stained with hematoxylin and eosin (H&E). The histological features were visualized and documented using a light microscope (Leica, DM2500, Germany). For immunohistochemical (IHC) staining, sections were heated in 0.1 M citric acid buffer at 98°C for 10 min, followed by blocking with 3% BSA. Sections were then incubated with antibody against CD68 (Arigo, ARG10514, China). For immunofluorescence analysis, primary antibodies against iNOS (Arigo, ARG56509, China) and CD206 (Arigo, ARG22456, China) were applied, followed by incubation with fluorochrome-conjugated secondary antibodies. Nuclei were counterstained with DAPI Fluor mount-G (SouthernBiotech, USA). Images were captured using a Leica DM2500 fluorescence microscope and analyzed using ImagePro Plus software. Each experiment included at least three samples from each group.

RT-qPCR analysis

Primer sequences are provided in Supplementary Table SI.

Western blot analysis

The following antibodies were used for western blot: AQP9 (Santa Cruz, sc-74409, 1:600), NOX2 (Santa Cruz, sc-130543, 1:500), phospho-IKKα/β (Abmart, TP56290, 1:2000), IKKα/β (Abmart, T55660, 1:2000), IκBα (Abmart, T55026, 1:2000), phospho-p65 (Abmart,

* Corresponding author: zhangbo@njucm.edu.cn, wangyan2020@njucm.edu.cn, matonghui@njucm.edu.cn
0030-9923/2024/0001-0001 $ 9.00/0

TP56372, 1:2000), p65 (Abmart, T55034, 1:2000), GAPDH (Proteintech, 10494-1-AP, 1:5000), Histone H3 (Proteintech, 17168-1-AP, 1:5000).

Supplementary Table SI. Primer sequences for RT-qPCR.

Gene	Primer Sequence (5′ → 3′)
Aqp9	F: GGGAGCCTTTGTCGGGGCTG
	R: ATGGGCTCCAGGCCTCTGGG
Il-1β	F: TGCCACCTTTTGACAGTGATG
	R: TGATGTGCTGCTGCGAGATT
Tnf-α	F: AAGCCTGTAGCCCACGTCGTA
	R: GGCACCACTAGTTGGTTGTCTTTG
Il-6	F: TAGTCCTTCCTACCCCAATTTCC
	R: TTGGTCCTTAGCCACTCCTTC
Il-10	F: CTTACTGACTGGCATGAGGATCA
	R: GCAGCTCTAGGAGCATGTGG
inos	F: CACCAAGCTGAACTTGAGCG
	R: CGTGGCTTTGGGCTCCTC
Cd206	F: CTCTGTTCAGCTATTGGACGC
	R: CGGAATTTCTGGGATTCAGCTTC
β-actin	F: CTGTGCCCATCTACGAGGGCTAT
	R: TTTGATGTCACGCACGATTTCC